SEMI-AUTOMATED DETERMINATION OF *TOXOPLASMA GONDII* LOCALIZATION IN THE CENTRAL NERVOUS SYSTEM

By

COLIN POTTER

A Thesis Submitted to The Honors College

In Partial Fulfillment of the Bachelor's degree
With Honors in

Neuroscience and Cognitive Science

THE UNIVERSITY OF ARIZONA

M A Y 2 0 1 8

Approved by:

Dr. Anita Koshy
Department of Neurology, Immunology

Abstract

I have studied the interactions between cells of the brain and the neurotropic parasite *Toxoplasma gondii*. Using an *in vivo* system that allows us to permanently mark and identify brain cells injected with *Toxoplasma* protein, we have identified that *Toxoplasma*-injected neurons (TINs) are heterogeneously distributed throughout the brain. Unfortunately, standard methods to quantify and map heterogeneous cell populations onto a reference brain atlas are time consuming and prone to user bias. We developed a novel MATLAB-based semi-automated quantification and mapping program to allow the rapid and consistent mapping of heterogeneously distributed cells on to the Allen Institute Brain Atlas. The procedure takes advantage of simple immunohistochemistry labeling techniques, use of a standard microscope with a motorized stage, and low cost computing that can be readily obtained at most research institutes. The system uses a two-threshold background subtraction to identify and quantify cells of interest, and automated transformation to align experimental images onto a brain atlas. We demonstrate that we reliably quantify and neuroanatomically localize TINs with low intra- or inter-observer variability. Additionally, we show that specific regions of the mouse brain are enriched with TINs after *T. gondii* infection. The discovery of TIN enrichment in specific brain regions was facilitated by our quantification method described here, which allowed reliable visualization, quantification, and mapping of TINs populations in immunolabeled sections across whole mouse brains.

1. Introduction

Toxoplasma gondii is an obligate intracellular parasite that naturally infects a wide range of warm blooded mammals, including humans and rodents, although felids are the parasite's definitive host (Dubey et al., 1998; Dubey 2008). In most hosts, *T. gondii* is able to establish a life-long infection in specific tissues, like cardiac, skeletal and nervous tissue. In humans and rodents, the central nervous system (CNS) is the major organ of *T. gondii* persistence (Dubey 1998, Remington & Cavanaugh, 1965). This tropism for and persistence in the CNS underlies the devastating symptomatic disease *T. gondii* causes in humans with under-developed immune responses (e.g. fetus, AIDS patients), which is characterized by widespread lesions in the brain parenchyma and retinopathy in adults and hydrocephaly in infants (Luft & Remington, 1992; McLeod et al., 2009). The persistent form of the parasite, the bradyzoite, is a slow-growing form that establishes intracellular cysts, primarily in neurons (Ferguson and Hutchinson, 1987; Melzer 2010; Cabral et al., 2016).

While *T. gondii* has a large number of strains types, the most studied are the three canonical strains, called type I, II, and III (Lorenzi et al., 2016). These three strain types were originally characterized by their acute virulence in mice with type I being hypervirulent, where infection with one parasite is sufficient to kill a mouse, type II has a middle range of virulence, and type-III is avirulent. Our understanding of *T. gondii*-CNS interactions has been primarily focused on the systemic immune response capable of keeping these parasite strains in check, leaving fundamental questions about parasite-neuron interactions unanswered. In particular, while it is known that *T. gondii* persists primarily in neurons, the factors that drive parasites to encyst in neurons, and which neuronal subtype, if any, are targeted are unknown. In an effort to address such gaps, we began to investigate the neuroanatomic localization of *T. gondii* interaction with neurons.

In the past, the most effective way to identify infected brain regions in mice was by cyst location. Several studies found that encystment is highest in the neocortex, thalamus, and striatum, along with other forebrain structures (Berenreiterová et al., 2011; Evans et al., 2014). However, cyst location does not necessarily give an accurate representation of which neurons or CNS regions are infected, as cysts can be located in distal processes > 100 microns from the neuron soma (Cabral et al., 2016). The development of a Cre-reporter system in which permanent host cell GFP-expression is triggered by injection of a Cre-fusion protein significantly changed this landscape (**Fig. 1**) (Koshy et al., 2012; Cabral et al., 2016). First, GFP expression leads to the ability to visualize the whole neuron (both cyst location and soma) (Koshy & Cabral, 2014). Second, as this system is dependent upon injection of a *T. gondii* effector protein, not active infection, it revealed that *T. gondii* injects its effector proteins—parasite proteins that hijack host cell processes and signals—into far more host cells than it productively infects (Koshy et al., 2012). This finding is particularly pronounced in the CNS, where *T. gondii*-injected neurons (TINs) out-number cysts up to 50-fold (Koshy et al., 2012). Thus, by mapping TINs, we can determine if cysts are commonly found in specific brain regions because these regions are particularly susceptible to *T. gondii* infection or if neurons display regional differences in the capability to clear intracellular parasites, as has been suggested for West Nile Virus (Cho et al., 2013). To test this hypothesis, we needed to reliably quantify and neuroanatomically localize TINs throughout the entire brain.

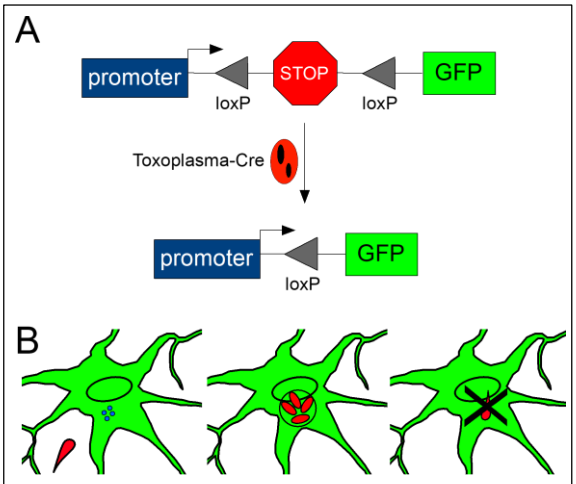

Figure 1. *Toxoplasma*-Cre allows permanent tracking of neurons injected with *Toxoplasma* proteins.
(**A**), Schematic of transgene carried by Cre reporter mice and the effect of injected Cre on recombination. (**B**), Options for how *Toxoplasma*-injected neurons arise. From left-to-right: failed invasion; active infection with cyst development; and active invasion followed by neuron killing of intracellular parasite (unknown mechanisms).

Until recently, processing large sets of data from whole-brain images has been time consuming and labor intensive as it required manual counts and manual identification of neuroanatomic location. To address this issue, various quantification methods have been developed. Stereological methods have allowed researchers to quantify cells in a precise stereotyped manner (Sterio 1984; Howard et al., 1998; Gundersen et al., 1986; West et al., 1991; Hedreen, 1998). These techniques were developed to count cells in relatively small sample regions of pre-identified neuroanatomic locations and in regions with uniform cell densities (Schmitz et al., 2005).

However, in *T. gondii* infection, TINs can be heterogeneously distributed throughout the brain and idiosyncratically vary between mice, thus establishing stereology parameters is difficult to accomplish since a vast number of areas would have to be sampled. In such situations, ideally, one would want to quantify and neuroanatomically map the cells of interest across the whole brain, across a number of mice and sample a wide range of tissue sections. Recently, there has been growing literature on imaging of whole brains or thick serial sections using a variety of imaging techniques like confocal imaging, 2-photon imaging, light-sheet microscopy and micro-optical sectioning tomography (Peng et al., 2017; Inglis et al., 2008). These imaging techniques have been used in combination with complex algorithms and machine learning techniques to localize and quantify cells. The equipment used and methods of quantification are not readily available at many universities, and manual counting of these large populations of TINs would be time-consuming and inefficient. Thus, the lack of large-scale, efficient methods to quantify and localize idiosyncratic cell distributions throughout a whole mouse brain section was an impediment to moving this work forward. To overcome this barrier, we developed a semi-automated method that can be utilized by most researchers because it relies on standard immunohistochemistry and basic light microscopy coupled to a MATLAB (Mathworks, Inc., Natick, MA)-based program to count and map cells of interest onto the Allen

Institute Mouse Brain Atlas (http://www.brain-map.org/). While the program has been developed for identifying TINs, it can be applied to count and localize a wide variety of cells or processes within histological images of sagittal mouse brain sections. After testing and verification of the program itself, we applied this semi-automated method to mouse tissue that had been *T. gondii* and quantified TINs throughout the entire mouse brain.

2. Methods

2.1 Animal and Parasite Model

The animal model used for these experiments is B6.Cg-Gt(ROSA)26Sort$^{m6(CAG-ZsGreen1)Hze}$/J on a C57BL/6J background (Madisen et al., 2010). The cells of these floxed-stop Cre reporter mice only express a green fluorescent protein (ZsGreen) after Cre-recombinase mediated genetic recombination. The *T.gondii* parasite strain used for this study was engineered to inject Cre into host cells concomitantly with parasite effector proteins (parasite proteins used to manipulate host cells) (Koshy et al., 2010; Koshy et al., 2012).

Parasites were maintained via serial passage through human foreskin fibroblasts using DMEM supplemented with 2 mM glutagro, 10% fetal bovine serum, and 100 I.U./ml penicillin/ 100 µg/ml streptomycin (Cabral, Tuladhar et al., 2016). Mice were infected at 2-3 months of age via intraperitoneal (IP) injection with freshly syringe-released parasites. Mice were inoculated with 10,000 parasites per 200 µl volume in USP grade PBS. At 3 weeks post infection, animals were sedated with a ketamine/xylazine cocktail, intracardially perfused with saline followed by 4% paraformaldehyde, after which brains were harvested.

2.2 Immunohistochemistry

Left and right brain hemispheres were isolated and sectioned in the sagittal plane at 40 microns on a sliding microtome. Sections were sampled every 200 microns to obtain a set of 20 sections, that would increase the likelihood of finding matching sections to the Allen Mouse Brain Atlas (ABA). Sections were pre-mounted on slides before immunohistochemical labeling (**Fig. 2**). Tissue was allowed to air-dry onto slides overnight and dehydrated using increasing then decreasing concentrations of 50%, 75%, 95%, and 100% ethanol to insure adhesion of tissue onto slides. Slides were washed with TBS, peroxidases inactivated (3%H_2O_2/10% methanol), permeabilized (0.6% Triton X-100), blocked (1.5% BSA and 1.5% goat serum), and incubated with Rabbit anti-ZsGreen (Clontech, Cat. No. 632474, 1:10,000) for 15-18hrs. Next, slides were incubated in Goat anti-rabbit polyclonal biotinylated conjugated antibody (Vector Labs, Cat. No. BA-1000, 1:500) for 2 hrs, incubated with avidin-biotin complex kit (ThermoFischer Scientific, Cat. No. 32020) for 2 hrs and visualized with a 3,3'-diaminobenzidine kit (Vectastain, Vector Labs Cat. No. SK-4100). Sections were then counterstained with cresyl violet for Nissl labeling (Dorph-Petersen et al., 2001). Although Nissl counterstain is not part of the colorimetric thresholds used in cell detection, clear Nissl staining aided in contrast between TINs and surrounding tissue, and allowed for identification of anatomical landmarks important for cell mapping. After processing tissue sections were estimated to shrink by 50%.

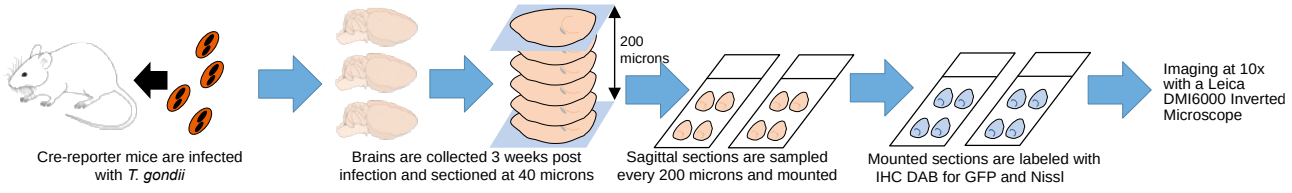

Figure 2. Histological workflow and imaging of brain tissue.
Mice were infected with either II-Cre or III-Cre parasites at inoculums of 10,000 parasites. Brains were then collected at 3 weeks post infection (wpi). Sections were sampled in 200 μm increments to increase the likelihood of matching sections from the sagittal Allen Mouse Brain Atlas (ABA). Appropriate sections were sampled at 1:5 and pre-mounted onto slides, and GFP antigen was visualized via immunohistochemistry using a standard DAB kit and counterstained with cresyl violet. The slides were then imaged on a Leica DMI6000 microscope with a motorized stage, and stitched images were collected with a 10x objective. The same imaging parameters were used across all slides for each experiment.

2.3 Microscopy

Slides were imaged on a Leica DMI6000 with a motorized stage, using Leica Application Suite X (LAS X). All images were taken with a 10x objective lens, the working distance of the objective used was sufficient to capture the whole depth of TINs. Base background subtraction and white balance was maintained throughout the same experiment to ensure consistent exposure. Image stitching was done automatically through LAS X with a 10% overlap. Images were stored as Leica Image File Format (lif).

2.4 Computer hardware and software specifications

All images were processed on a computer with an Intel 6-core 6800k processor with 32GB of RAM. The operating system used was Windows 10 Professional. All MATLAB code was written and run using MATLAB 2015a.

2.5 Cell detection and counting

Individual histology section images were imported into MATLAB and TINs were automatically identified using colorimetric and size thresholds (**Fig. 3A**). Immunohistochemistry used to stain TINs brown caused some clearly visible regional light brown staining of the background due to high background labeling. Consequently, TINs in these regions consistently stained darker than those that were on unstained background. To make segmentation of the TINs simpler, the background was separated into two regions—light brown stained and unstained background (**Fig. 3 B/B'**). This was done by using a color threshold to segment the light brown region of the tissue. The threshold was manually-selected and was tested across different tissue sets. A series of erode and dilate functions were used to remove small objects outside the light brown region and to make the light brown region contiguous. The complementary region was used as the unstained tissue background region. Both regions were

dilated slightly so they would overlap to account for minor region segmentation error. This would account for TINs that may have been located on region border or be located slightly outside the

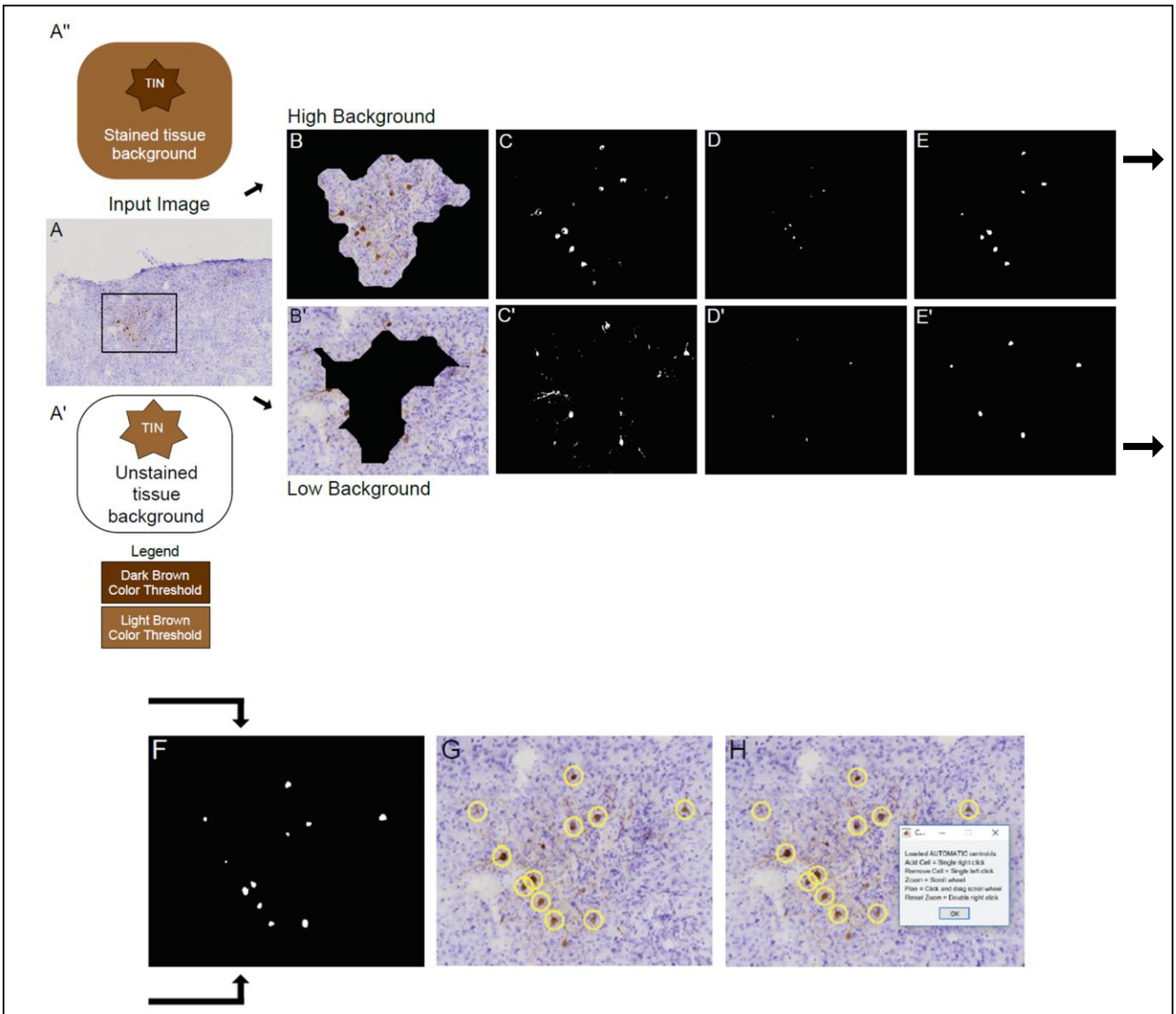

Figure 3: Workflow of MATLAB cell detection and quantification includes separation of image into areas of high and no brown background staining.
(**A**) Original image. Top schematic shows how TINs stain dark brown when in area with high brown background staining (**A''**). Bottom schematic shows how TINs stain light brown in area with no brown background staining (**A'**). Experimental image (**A**) is split into two regions through RGB thresholds: Light brown regions from high brown background labeling (top row, **B**) and regions with no brown background staining (bottom row, **B'**). Separate RGB color thresholds are applied to each region to generate a Boolean mask of DAB+ regions (**C**, **C'**). Perimeter of shapes is eroded to remove irregular shapes (**D**, **D'**), then dilated back to original size (**E**, **E'**). The two masks are combined for final quantification (**F**). Regions are marked with centroids (**G**), and operators use a dialog box to manually error-check identified cells (**H**).

intended region. Segmentation of the TINs and background by color is summarized in the (**Fig. 3 A' & A''**).

In the light brown background regions, TINs were consistently stained dark brown. ImageJ was used to measure the RGB values of several manually-selected TINs. These RGB values were used to threshold and segment the TINs. TINs in the unstained tissue region were light brown and segmented with the same methods. Small, non-circular objects (e.g. processes) were removed with a sequence of erode functions (**Fig. 3 C/C', D/D'**). The remaining segmented objects (TINs) were dilated to their original diameter (**Fig. 3 E/E'**). A size threshold was used to remove objects that were larger than cells. The light and dark brown segmented TINs were merged to eliminate double-counting in the overlapping regions. Overlap in light and dark brown masks was added to assist in identification of borderline cells, and differences when changing mask overlap are demonstrated in (**Fig. 4C, F**). The TIN centroids were automatically encircled on the section image (**Fig. 3 F, G**). The analyzed image was then manually corrected

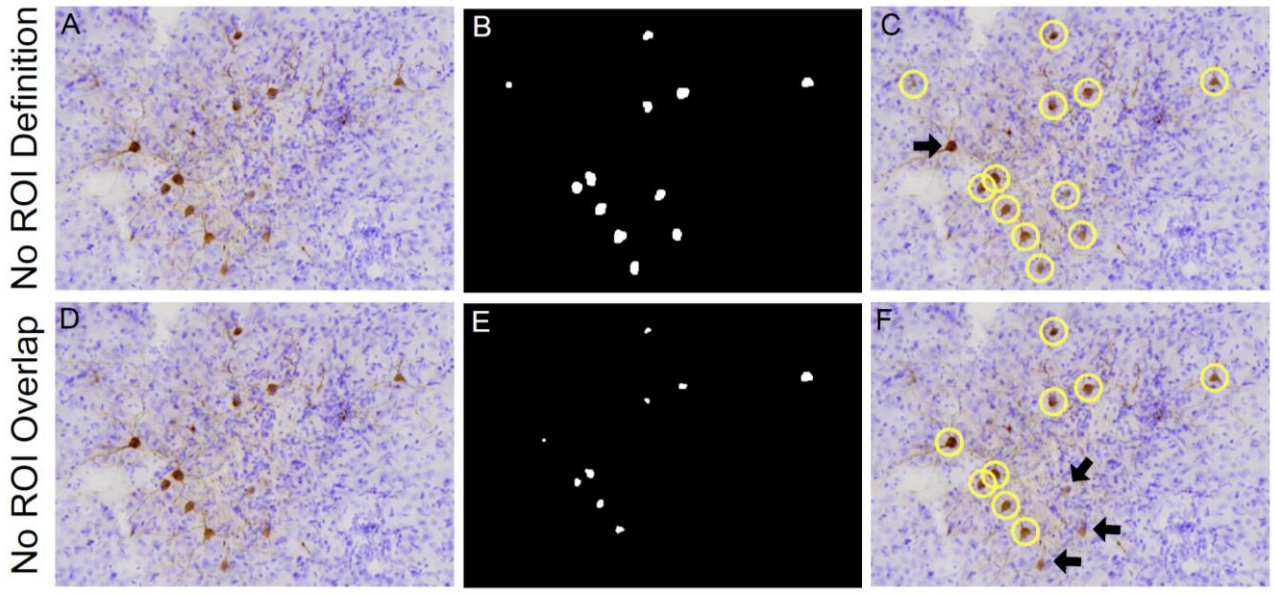

Figure 4: Program mis-counts TINs when not adjusting for background or with no mask overlap.
(**A**) Original image. (**B**) Mask generated when applying single RGB threshold to tissue with varying background. (**C**) TINs identified by program with this work flow. Black arrows identify TINs missed by this single RGB threshold program. (**D**) Original image that is separated into high background and no background areas (Fig. 2). (**E**) Mask generated when separated areas are re-merge without overlap. (**F**) TINs identified by program using nonoverlapping merge. Black arrows identify TINs missed by this work flow.

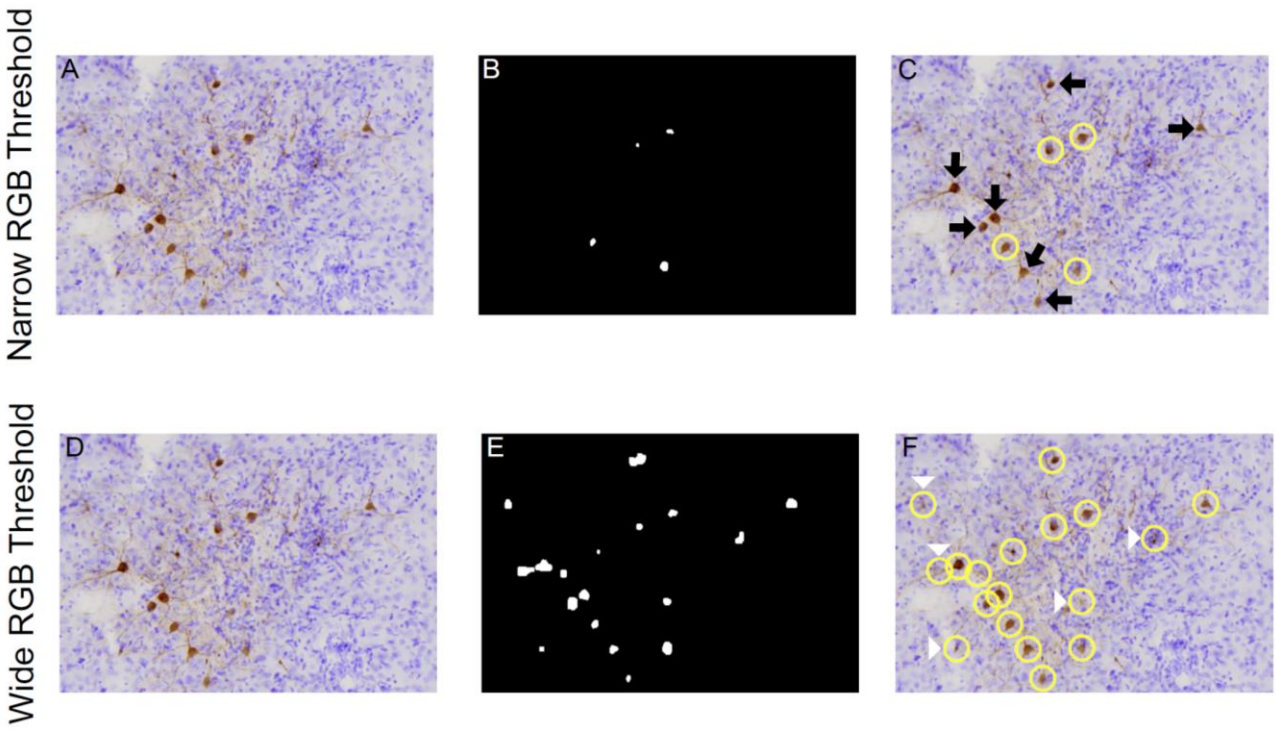

Figure 5: Adjustment of RGB thresholding affects accuracy of quantified TINs.
(**A, D**) Original image. (**B**) Mask generated by narrowing RGB threshold by 40%. (**C**) TINs identified using these narrow RGB thresholds. Black arrows identify TINs missed by this narrow threshold (increased false negatives). (**E**) Mask generate by broadening RGB threshold by 40%. (**F**) TINs identified using broad RGB thresholds. White arrowheads identify non-TINs that have been quantified (increased false positives).

(i.e. unmarked TINs were marked and false positive TINs were unmarked) using a custom-built graphical user interface that allowed for rapid selection and removal of cells. The selected RGB threshold values erred towards overcounting TINs (i.e. false-positive TIN detection) as it was more efficient to remove incorrectly identified cells than to examine the whole section and identify uncounted TINs (i.e. false-negative TIN detection) if the RGB values were too stringent. To demonstrate this point, a decrease in the RGB threshold range values by 40% led to a decrease in TIN centroids (**Fig. 5C**), while an increase in the threshold value range by 40% increased the number of TIN centroids and false positive cell bodies (**Fig. 5F**). The RGB threshold values used were determined empirically and gave reliable results across different tissue sets.

2.6 Image registration

Mapping of brain section images to the Allen Brain Atlas (ABA) was accomplished in a multi-step process. First, 20 sagittal atlas images were downloaded as vector images (in SVG format). Each anatomical region was outlined with black lines. The outlines were removed using Inkscape software (Albert, M., et al. "Inkscape." 2015) and the images were saved as pixelated images. A set of 20 corresponding reference infected brain tissue section images (referred to as reference images from here forward) were imported into MATLAB using the Open Microscopy Environment Consortium's Bio-Formats software library (Linkert et. al., 2010). Pairs of corresponding reference and atlas images were then registered with an affine transformation (translation, rotation, scale, and shear) followed by a piecewise transformation using the MATLAB control point registration tool. Approximately 30 control points were manually placed on identical anatomical landmarks in the reference and atlas images, with emphasis on the tissue borders as well as internal structures. Empirical testing of brain landmarks that gave the best fits led to exclusion of control points on the olfactory bulb and cerebellum. The transformation matrices generated by the control point registration were saved so they could be used in subsequent processing steps. While this procedure required a significant amount of user interaction, it only had to be done once. New, experimentally generated labeled brain section images were registered to the untransformed reference brain section images with an automatic affine transformation. Finally, all the brain section images were warped using the saved transformation matrices so that all experimental sections were aligned to the atlas images. Registration alignment for brain section images were visually inspected by overlaying individual images to the corresponding atlas image (**Fig. 6**). The number of TINs in 12 major anatomical regions of the brain was determined using the TIN centroids and Boolean masks for each region of the brain identified in the atlas image. In the atlas images, each anatomical

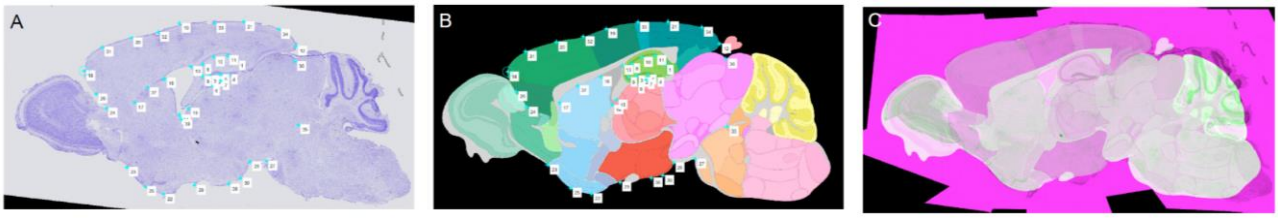

Figure 6: Image registration of brain sections onto atlas image.
(**A**) Anatomical control points on reference image 14 corresponding to control points on Allen Mouse Brain Atlas (**B**). (**C**) Output transformation of (**A**) onto (**B**) from cell mapping program.

region has a defined color. Masks for each anatomical region were created by isolating an SVG image and isolating each colored region.

2.7 Validation

Intra-operator and inter-operator variability were assessed to determine the reliability of our program. Intra-operator analysis was conducted by comparing the semi-automated program results between two independent sessions with the same operator. A single operator used the program to count cells in 3 sets of tissue, each consisting of 20 sections. The same operator counted the same 3 sets of tissue during a second counting session two days later. To assess variability between sessions, the coefficient of variation (CV) was calculated for the total cell counts of each set independently by dividing the standard of deviation of the cell counts by their mean value (SD/Mean). The average CV was calculated between sets to take all sets into account. To assess cell-mapping consistency, counts from Set 1 were broken down into major brain regions to compare the number of cells localized to each region between different sessions.

Assessment of inter-operator error was carried out by comparing the total cell counts between two operators counting the same 3 sets of tissue in independent sessions without a supervisor. The CV was calculated for each set independently and averaged, similar to intra-

operator analysis. Set 1 was split into major brain regions to compare cells localized to each region for different operators.

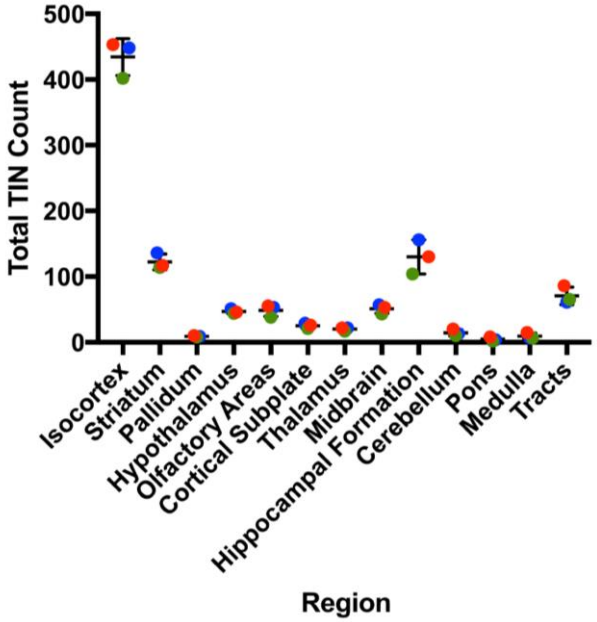

Figure 7: TIN quantification and mapping by program (uncorrected) compared to manual count by two independent users.
Program quantification is shown from a single mouse and 20 sections total were quantifed. Program quantification parameters are set to overcount since deleting centroids was determined to be faster when using the GUI to ensure proper quantification. Blue colored dots represent uncorrected counts after program is run. Green and red dots represent manual counts from two users correcting the program quantification. In some cases like in the isocortex one user may overcount, but from previously shown data we found that the variance among users is low.

3. Semi-automated Program Verification

3.1 False-positive and false-negative rates

We designed our program to err towards overcounting our manual counts, since we found deleting points easier to delete than manually adding with the GUI. Two separate users sampled tissue sections from one mouse and compared counts to the uncorrected output by the program. Here we demonstrate that our program tends to overcount across most regions of the brain across users with little variability (**Fig. 7**).

Table 1 demonstrates that user 1 compared to uncorrected quantification had a range count across specific regions of the brain from -26 to +25. Compared to user 2 the unaided quantification ranged from +2 to +52, demonstrating that for most regions of the brain the program tended to err towards overcounting within the range of user variability.

3.2 Intra-operator and inter-operator validation

The average coefficient of variation (CV) across all 3 sets of tissue for intra-operator analysis was 4.97% (**Fig. 8A**). Comparison of cell localization data by major brain regions

between sessions shows similar values in each of the major brain regions, with an average difference of 8 cells in each region (**Fig. 8B**). Low variation in overall cell quantification and in localization between sessions indicates effectiveness and consistency of the semi-automated quantification method between different sessions with the same operator.

To further validate our system, we wanted assurance that our quantification was reliable across operators. An average CV of 1.68% for inter-operator variation was calculated across all 3 quantified sets (**Fig. 8C**). A comparison of cell counts by major region also shows similar values across these regions, with an average difference of 10 cells (**Fig. 8D**), indicating an accuracy of cell quantification and localization between different operators.

To further quantify the variation in intra-operator and inter-operator regional counts, each counting session was plotted against each other (**Fig 9**). Each regression line had an r^2 value of .998, indicating that regionalization using this method is highly consistent for both intra-operator and inter-operator counts.

Table 1: TINs mapping from two independent users compared to uncorrected counts generated by automated program.

Users sampled sets of tissue that corresponded to specific Allen atlas sections. Final outputed centroids were corrected since by users since output parameters are set to overcount TINs. For user 1 quantification of final counts compared to uncorrected program counts range from -26 to +25. For user 2 final count differences ranged from +2 to +51.

Region	User 1	User 2	No correction	+/- from User 1	+/- from User 2
Isocortex	448	402	453	5	51
Striatum	136	114	117	-19	3
Pallidum	9	8	10	1	2
Hypothalamus	51	44	46	-5	2
Olfactory Areas	53	38	55	2	17
Cortical Subplate	29	21	26	-3	5
Thalamus	22	17	22	0	5
Midbrain	57	43	53	-4	10
Hippocampal Formation	156	104	130	-26	26
Cerebellum	13	10	20	7	10
Pons	4	2	8	4	6
Medulla	7	7	15	8	8
Tracts	61	65	86	25	21

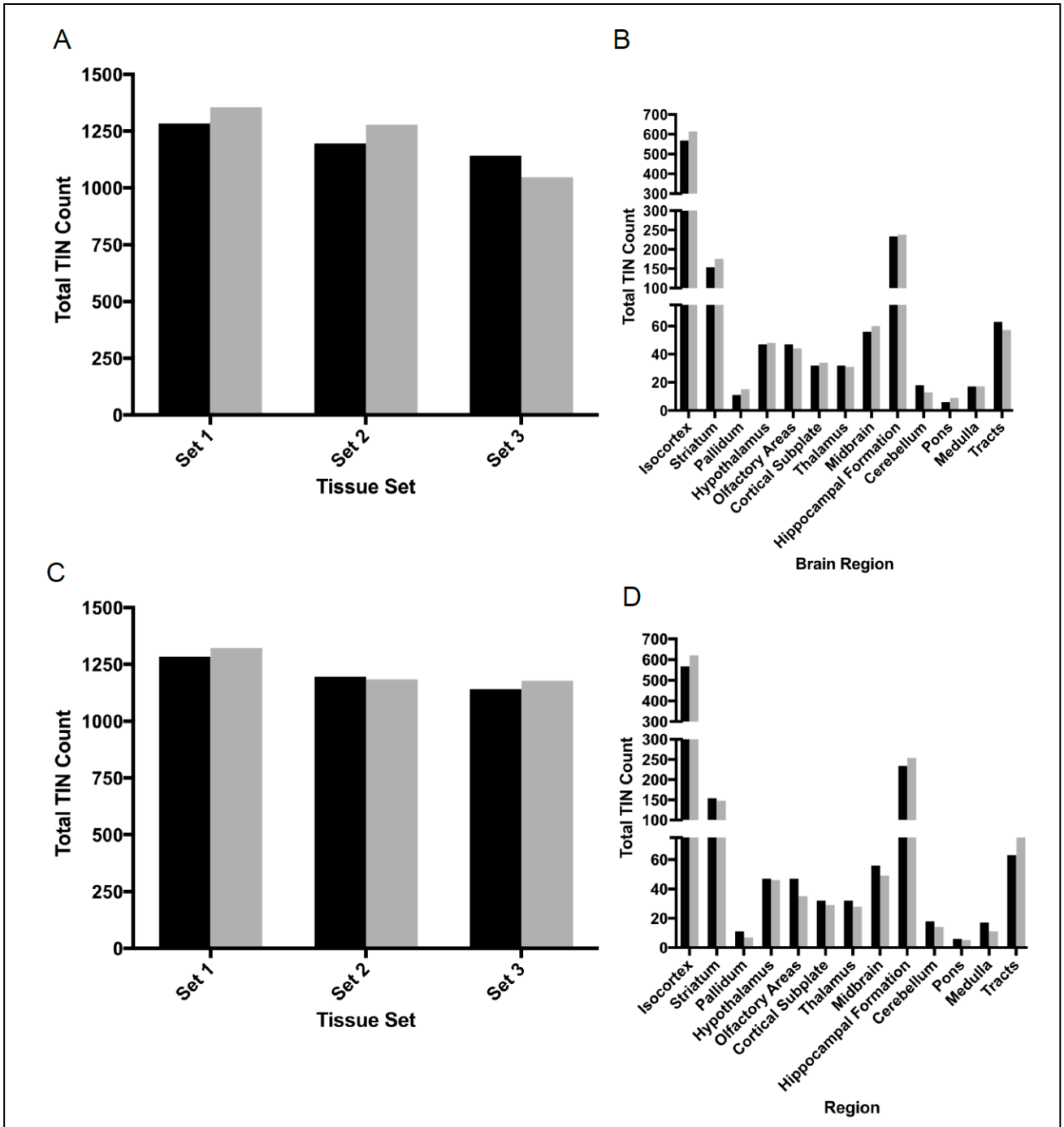

Figure 8: Quantification and validation of semi-automated program.
Three weeks after infection with parasites, a brain was harvested, sectioned, sampled, and stained as previously outlined. TINs were quantified from 3 sets of tissue from this brain. (**A**) Intra-operator cell counts in 2 independent experiments for 3 different tissue sets. Coefficient of variation was 3.80%, 4.63%, and 6.20% for Sets 1, 2, and 3 respectively, and the average was 4.97%. Low variation indicates that the program is reliable between experiments with the same operator. (**B**) Intra-operator cell counts for Set 1 broken down into major mouse brain regions. Low variation indicates regional consistency in cell counting, and consistency in semi-automated mapping. (**C**) Inter-operator cell counts for 3 different tissue sets. Cells were counted in the absence of a supervisor to eliminate unintentional bias. The coefficient of variation was 2.06%, 0.77%, and 2.19% for Sets 1, 2, and 3 respectively, for an average coefficient of variation of 1.68%. (**D**) Inter-operator cell counts for Set 1 broken down into the major mouse brain regions which showing low regional variability. N = 1 mouse.

3.3 Software efficiency and viability

Compared to manual counting, semi-automated counting is significantly faster. After imaging was completed, quantification and mapping of TINs from 6 mice, each with 16-20 whole-sections, was completed in less than a week, with automated counting and image registration running overnight. This indicated a nearly 3-fold increase in tissue processing capability when compared to manual counting and mapping of experimental tissue. Automatic image counting time ran from 32 seconds on smaller images to 108 seconds on larger images, and image transformation generally ran from 76 - 139 seconds, which was dependent on the image size. GUI-assisted counting was the longest step in the protocol, each section taking on average 6-7 minutes.

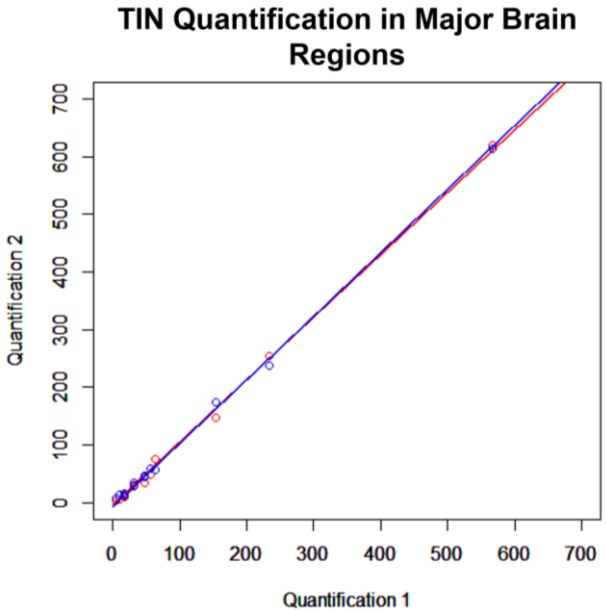

Figure 9: Regression showing regionalization counts from intra-operator and inter-operator analysis. Blue shows regression line for intra-operator regional counts plotted session 2 vs session 1. r^2 value for this correlation was .998. Red indicates the regression line for inter-operator counts plotted operator 2 vs operator 1. r^2 for this correlation was .998. This indicates that there was very little variability in each of these data and semi-automated regionalization is reliable.

4. TIN Localization in the Mouse Brain

4.1 Determination of TIN regionalization

To apply this semi-automated method, 12 Cre-reporter mice were infected with type-II *T. gondii*-Cre parasites for 3 weeks, after which brains were harvested and tissue was processed and analyzed using the semi-automated method. Sections sampled for these mice ranged from 16-20 sections, a full set of 21 sections was not possible for all animals because of variability

from sectioning. Raw cell counts obtained from our program showed high numbers of TINs in the isocortex and striatum (**Fig. 10A**). Further analysis was needed to determine if these high numbers were a result of higher brain area of these regions and thus a random TIN distribution, or whether parasites were preferentially interacting with neurons in these regions over other regions. To account for the possibility of a random distribution of TINs, raw counts were normalized to the area of each brain region across all ABA sections (**Fig. 10B**). Normalization revealed that, indeed, the cortex and striatum were enriched with TINs compared to other brain regions, and also revealed that the pallidum was enriched for TINs and, interestingly, that the cerebellum was largely devoid of TINs across all animals.

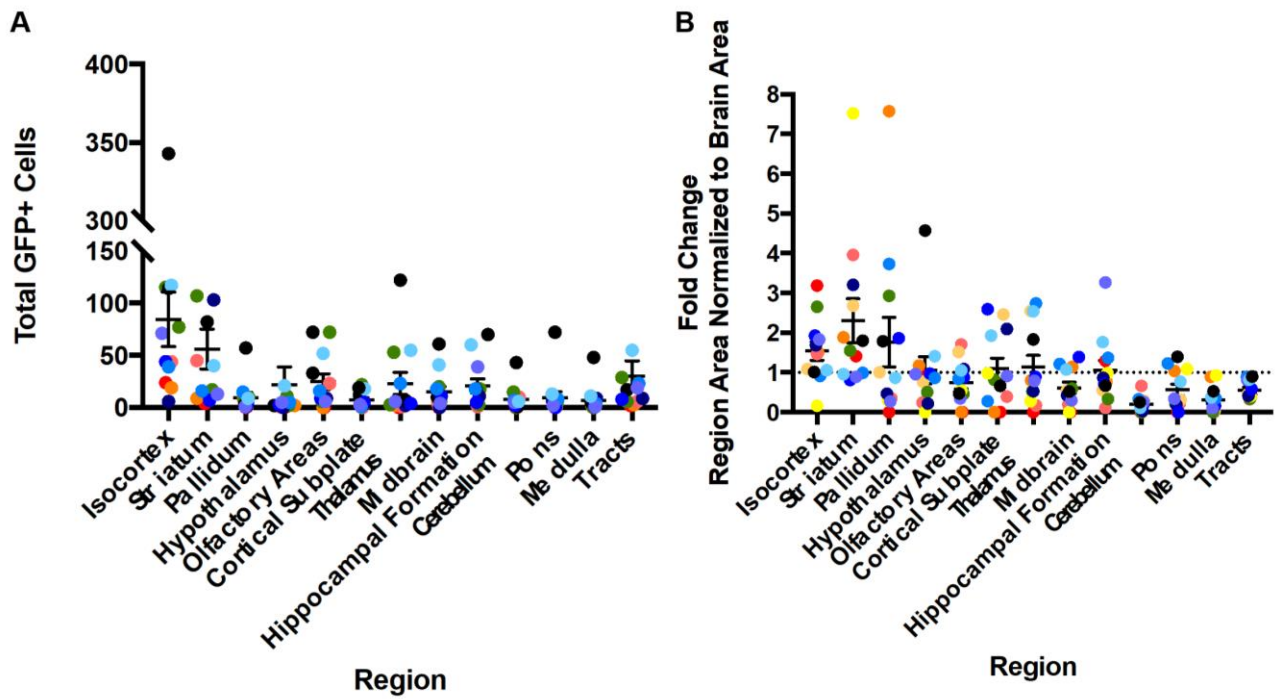

Figure 10: TIN localization in the mouse brain.
(**A**) Raw cell quantification of TINs using the semi-automated method and broken up into major brain region. Quantified cells were seen most often in the cortex and striatum. (**B**) Area-based normalization of raw TIN counts from (**A**). Area normalization was performed by comparing the proportion total observed TINs that were in a particular brain region to expected proportion of TINs that should be in that same brain region based on the proportion of area that region encompasses on the ABA. Values above 1 indicate enrichment of TINs in a particular brain region, and values lower than 1 indicate proportional absence of TINs.

5. Discussion

We have developed a unique semi-automated cell quantification and localization protocol. This method allows operators to obtain total cell counts across a whole-brain section throughout the entire brain within a 5 percent variation between trials and operators, effectively eliminating most of the subjectivity associated with manual counting. We implemented this method and were able to effectively quantify and localize TINs in the mouse brain. The low variability in the intra- and inter-operator quantification indicates reliable, reproducible data acquisition between different sessions and different users. While this approach was shown to be effective for identifying TINs, this method can be adapted to quantify and localize other immunolabeled cells or plaques and aggregates from AD models by changing the parameters the program utilizes when delineating cells from non-cells. Our MATLAB code can also be modified to quantify large sets of images in fluorescent tissue as well. Coding in MATLAB allows these parameters to be altered easily with trial-and-error refining of these parameters. Additionally, this method could be utilized to quantify large, non-homogeneous cell populations in the spinal cord or any other organ, provided an atlas exists for the organ of interest, as a new reference atlas could be generated. This is especially useful if little or no data exists about localization of a particular cell or aggregate of interest.

This method provides accurate data with minimal set up and investment in time. Recently, other methods have been established to count and localize cells in the brain, but these methods require access to high-end equipment, computing resources and dedicated computer science departments that are often unavailable at smaller research institutions. Our method is carried out using a relatively low-cost computer, a standard version of MATLAB, and a microscope with a motorized stage with image stitching capabilities, all of which are commonly available even at smaller universities. This semi-automated method is a valuable approach to first-steps quantification and localization of immunolabeled objects and overall provides

accurate and consistent results using basic laboratory equipment and computing, making it a fast and versatile way to quantify cells.

Additionally, we have found that there seem to be specific brain regions where *Toxoplasma gondii* interacts preferentially with neurons. This raises the possibility that *T. gondii* targets specific neural subtypes present in these regions for interaction and infection. If this is the case, it would allow us to begin to investigate the mechanisms underlying the parasite's invasion process, and the effect that it has on neural processes. To assess the extent of neural subtype colocalization, immunofluorescence labeling for subtype markers can be combined with confocal imaging to visualize colocalization of TINs with these subtype markers. It is also possible that this regionalization is due entirely to differences in where the parasite is able to penetrate into the brain parenchyma as a result of differences in blood brain barrier (BBB) permeability in affected versus unaffected regions. To test this possibility, perfusion with Evans Blue (EB) dye would be sufficient to visualize BBB leakiness. If such perfusion is done at different time-points after infection, the progression of leakiness can be visualized and the distance between focal points of BBB leakiness and nearby TINs can be measured in thick sections using confocal microscopy. This experimental design will allow us to determine the likelihood that BBB composition in specific regions is a determining factor on TIN localization in the brain.

Acknowledgements

I would like to thank Oscar Mendez for his mentorship and work with me on this project, Anita Koshy for her mentorship and support, Elizabeth Fernandez for aiding in the cell detection script, and Carla Cabral for initial tissue sets used in these experiments. I would also like to thank the additional members of the Koshy and Trouard groups for helpful discussion of the methods and manuscript. Finally, thank you to the Neuroscience and Cognitive Science

Program and the Undergraduate Biology Research Program for their support. Funding was provided by the National Institute of Neurologic Disorders and Stroke R01 NS095994 (AAK), supplemental funding 01S1 (OAM) and the Arizona Biomedical Research Commission ADHS14-082991 (AAK).

References:

Sterio DC. The unbiased estimation of number and sizes of arbitrary particles using the disector. J Microsc 1984;134:127 – 36.

Howard CV, Reed MG. Unbiased Stereology: Three-Dimensional Measurement in Microscopy. Springer Verlag, 1998. pp. 1 – 19, 69 – 106, 151 – 176.

Gundersen HJ. Stereology of arbitrary particles: A review of unbiased number and size estimators and the presentation of some new ones, in memory of William R. Thompson. J Microsc 1986;143:3 – 45

West MJ, Slomianka L, Gundersen HJ. Unbiased stereological estimation of the total number of neurons in the subdivisions of the rat hippocampus using the optical fractionator. Anat Rec 1991;231:482 – 97.

Hedreen JC. Lost Caps in Histological Counting Methods. Anat Rec 1998;250:366 – 372.

Schmitz C, Hof PR. Design-Based Stereology in Neuroscience. Neuroscience 2005;130:813 – 31.

Peng J, Long B, Yuan J, Peng X, Ni H, Li X, Gong H, Luo Q, Li A. A quantitative analysis of the distribution of CRH neurons in whole mouse brain. Frontiers in neuroanatomy 2017;11:63.

Inglis A, Cruz, L, Roe DL, Stanley HE, Rosene DL, Urbanc B. Automated identification of neurons and their locations. Journal of Microscopy 2008;230(3):339-352.

Liebmann, T., Renier, N., Bettayeb, K., Greengard, P., Tessier-Lavigne, M. and Flajolet, M., 2016. Three-dimensional study of Alzheimer's disease hallmarks using the idisco clearing method. *Cell reports*, *16*(4), pp.1138-1152.

Dubey JP, Lindsay DS, Speer CA. Structures of *Toxoplasma gondii* Tachyzoites, Bradyzoites, and Sporozoites and Biology and Development of Tissue Cysts. Clin Microbio Rev 1998;11(2):267 – 99.

Dubey JP. The history of Toxoplasma gondii–the first 100 years. J Eukaryot Microbiol 2008;55: 467 – 75.

Remington, Jack S., and Ellen N. Cavanaugh. "Isolation of the encysted form of Toxoplasma gondii from human skeletal muscle and brain." *New England Journal of Medicine* 273.24 (1965): 1308-1310

Luft, B. J. & Remington, J. S. Toxoplasmic encephalitis in AIDS. *Clin. Infect. Dis.* **15,** 211–222 (1992).

McLeod, R., Kieffer, F., Sautter, M., Hosten, T. & Pelloux, H. Why prevent, diagnose and treat congenital toxoplasmosis? *Mem. Inst. Oswaldo Cruz* **104,** 320–344 (2009).

Ferguson DJ, Hutchinson WM. An ultrastructrual study of the early development and tissue cyst formation of Toxoplasma gondii in the brains of mice. Parasitology Research 1987;73:483-91.

Melzer, T.C., Cranston, H.J., Weiss, L.M. and Halonen, S.K., 2010. Host cell preference of Toxoplasma gondii cysts in murine brain: a confocal study. *Journal of neuroparasitology*, *1*.

Cabral C, Tuladhar S, Dietrich HK, Nguyen E, MacDonald WR, Trivedi T, Devineni A, Koshy AA. Neurons are the Primary Target Cell for the Brain-Tropic Intracellular Parasite *Toxoplasma gondii*. PLoS Path 2016;12(2):e1005447

Lorenzi H, Khan H, Behnke MS et al., Sibley LD. Local admixture of amplified and diversified secreted pathogenesis determinants shapes mosaic *Toxoplasma gondii* genomes. Nature Communications 2016; DOI: 10.1038/ncomms10147

Berenreiterová M, Flegr J, Kuběna AA, Němec P. The Distribution of *Toxoplasma gondii* Cysts in the Brain of a Mouse with Latent Toxoplasmosis: Implications for the Behavioral Manipulation Hypothesis. PLoS ONE 2011;6(12);e28925

Evans AK, Strassmann PS, Lee I-P, Sapolsky RM. Patterns of *Toxoplasma gondii* cyst distribution in the forebrain associate with individual variation in predator odor avoidance and anxiety-related behavior in male Long-Evans rats. Brain Behav Immun 2014;37:122 – 33.

Koshy AA, Fouts AE, Lodoen MB, Alkan O, Blau HM, Boothroyd JC. Toxoplasma secreting Cre recombinase for analysis of host-parasite interactions. Nat Methods 2010;7:307 – 9.

Koshy AA, Dietrich HK, Christian DA, Melehani JH, Shastri AJ, Hunter CA, Boothroyd JC. *Toxoplasma* Co-opts Host Cells It Does Not Invade. PLoS Path 2012;8(7):e1002825

Koshy, Anita A., and Carla M. Cabral. "3-D imaging and analysis of neurons infected in vivo with Toxoplasma gondii." *Journal of visualized experiments: JoVE* 94 (2014).

Cho, Hyelim, et al. "A role for Ifit2 in restricting West Nile virus infection in the brain." *Journal of virology* 87.15 (2013): 8363-8371.

Madisen L, Zwingman TA, Sunkin SM, Oh SW, Zariwala HA, Gu H, et al. A robust and high-throughput Cre reporting and characterization system for the whole mouse brain. Nat Neurosci. 2010;13:133 – 140.

Dorph-Petersen KA, Nyengaard JR, Gundersen HJG. Tissue shrinkage and unbiased stereological estimation of particle number and size. Journal of Microscopy 2001;204(3):232-246.

Linkert, M., Rueden, C.T., Allan, C., Burel, J.M., Moore, W., Patterson, A., Loranger, B., Moore, J., Neves, C., MacDonald, D. and Tarkowska, A., 2010. Metadata matters: access to image data in the real world. *The Journal of cell biology*, *189*(5), pp.777-782.